

Chapter 1

A Constitutive Description of Nonlinear Metamaterials Through Electric, Magnetic, and Magnetoelectric Nonlinearities

Stéphane Larouche, Alec Rose and David R. Smith

Abstract Nonlinear metamaterials provide a host of interesting phenomena which, like for their linear counterpart, can be described using homogenized, effective properties. Following the convention used in nonlinear optics, the response of nonlinear metamaterials can be expressed as a power series of the incident fields. However, contrarily to most materials used in nonlinear optics that only possess an electric nonlinear response, nonlinear metamaterials often show electric, magnetic, and magnetoelectric nonlinear responses within a single unit cell. In this chapter, we present two complementary approaches to determine all the effective nonlinear susceptibilities of nonlinear metamaterials. First we present a coupled-mode theory that provides insight into the origin of the various nonlinear susceptibilities that arise in nonlinear metamaterials according to the symmetry of the unit cell. This approach also leads to a description of the effect of the finite size of the unit cells, often called spatial dispersion. Second, we present a retrieval approach based on transfer matrices that can be used to determine the effective nonlinear susceptibilities from either simulated or experimental results. We finally demonstrate how to use this approach by applying it to the case of dual-gap varactor-loaded split ring resonators.

1.1 Introduction

Nonlinear metamaterials offer promising opportunities for enhancing and controlling nonlinear response. As discussed in the other chapters of this book, many interesting and unique nonlinear phenomena have been demonstrated using metamaterials, illustrating the potential for structured metamaterials to support novel

S. Larouche (✉) · A. Rose · D.R. Smith
Center for Metamaterials and Integrated Plasmonics, Duke University,
Durham, NC 27708, USA
e-mail: stephane.larouche@duke.edu

A. Rose
e-mail: arose@evolvetechnology.com

D.R. Smith
e-mail: drsmith@ee.duke.edu

nonlinear response not easily realizable in conventional materials. The design of nonlinear metamaterials, as has been the case for their linear counterparts, is greatly facilitated by the introduction of a homogenization scheme, wherein effective nonlinear susceptibilities for a composite are determined, in addition to the linear permittivity and permeability. The homogenization approach allows the anticipated properties of the nonlinear metamaterial to be determined efficiently from simulations of the repeated metamaterial element.

One of the advantages that has propelled the field of linear metamaterials is the expanded palette of available material response, including the capability of implementing electric, magnetic and magnetoelectric properties, even in the absence of inherently magnetic materials. The addition of magnetic response in metamaterials leads to a considerably rich and complex collection of phenomena, especially when magnetic nonlinearity is included. The issue of magnetoelectric coupling, in fact, arises naturally for nonlinear metamaterials, and thus nonlinear homogenization schemes must include and quantify a significantly larger set of nonlinear susceptibilities, the majority of which are negligible for conventional materials.

In this chapter, we present two complementary approaches to determine the homogenized, effective nonlinear susceptibilities of nonlinear metamaterials. First, we present a coupled mode theory that can be used to determine the effective nonlinear susceptibilities of simulated, lossless metamaterials. This method is particularly useful in deriving analytical formulas that provide insight into the origins of the various nonlinear susceptibilities that arise from the metamaterial elements and leads quite naturally to several important symmetry considerations. Second, we present a retrieval approach based on transfer matrices that can be applied to either simulation or experimental results, and is relevant for all scenarios that satisfy the non-depleted pump approximation. The insight provided by the coupled mode theory approach provides a basis for understanding the role that the symmetry of a metamaterial unit cell plays in determining which effective nonlinear susceptibilities can be supported by the homogenized metamaterial. This analysis also incorporates the effects of spatial dispersion due to the finite metamaterial element on the retrieved nonlinear susceptibilities. We illustrate the retrieval approaches using simulations on symmetric and antisymmetric dual-gap varactor-loaded split ring resonators, which have been used over the past several years to form analog nonlinear metamaterials at microwave frequencies.

Following the convention used in nonlinear optics, the nonlinear response of metamaterials can be expressed as a power series in the incident fields. To keep the number of terms tractable, we consider here only second order processes: 3-wave mixing where a field at ω_3 is generated by applying two fields at ω_1 and ω_2 . The methods presented here can trivially be expanded to include higher order processes. For the case of 3-wave mixing, the nonlinear polarization and magnetization at ω_3 can depend on either the electric or the magnetic field at ω_1 and ω_2 , which we indicate by dividing the nonlinear response in a series of nonlinear susceptibilities $\chi_{ijk}^{(2)}$ where i, j , and k can be either e or m . The first subscript indicates if the nonlinear susceptibility generates a nonlinear polarization or magnetization at ω_3 , while the

two other subscripts indicate whether this nonlinear polarization or magnetization is created by the electric or the magnetic field at ω_1 and ω_2 . Various nonlinearities generally coexist in a single metamaterial unit cell and it is necessary to devise a method to separate their effects.

It will be seen that for 3-wave mixing there are eight different nonlinear susceptibilities. In general, for an n th order process there are $(n + 1)^2$ nonlinearities present. Furthermore, each of these nonlinearities is a rank-3 tensor. By carefully applying the fields at ω_1 and ω_2 in various axes and polarizations, and determining the fields generated at ω_3 , it is possible to separately determine each element of these tensors, providing a full description of the nonlinear properties of the metamaterial.

1.2 Effective Nonlinear Susceptibilities: Coupled Mode Theory

In the most general case, the nonlinear properties of a material must take into account not only electric-dipole contributions, but also magnetic-dipole, quadrupole, and so-on. If we assume only dipolar contributions, we can write the second-order polarization through a series of nonlinear susceptibilities,

$$\begin{aligned} \mathbf{P}^{(2)}(\omega_3) = & \bar{\chi}_{eee}^{(2)}(\omega_3; \omega_1, \omega_2) : \mathbf{E}(\omega_1)\mathbf{E}(\omega_2) + \bar{\chi}_{emm}^{(2)}(\omega_3; \omega_1, \omega_2) : \mathbf{H}(\omega_1)\mathbf{H}(\omega_2) \\ & + \bar{\chi}_{eem}^{(2)}(\omega_3; \omega_1, \omega_2) : \mathbf{E}(\omega_1)\mathbf{H}(\omega_2) \\ & + \bar{\chi}_{eme}^{(2)}(\omega_3; \omega_1, \omega_2) : \mathbf{H}(\omega_1)\mathbf{E}(\omega_2), \end{aligned} \quad (1.1)$$

and the second-order magnetization,

$$\begin{aligned} \mu_0 \mathbf{M}^{(2)}(\omega_3) = & \bar{\chi}_{mmm}^{(2)}(\omega_3; \omega_1, \omega_2) : \mathbf{H}(\omega_1)\mathbf{H}(\omega_2) + \bar{\chi}_{mee}^{(2)}(\omega_3; \omega_1, \omega_2) : \mathbf{E}(\omega_1)\mathbf{E}(\omega_2) \\ & + \bar{\chi}_{mme}^{(2)}(\omega_3; \omega_1, \omega_2) : \mathbf{H}(\omega_1)\mathbf{E}(\omega_2) \\ & + \bar{\chi}_{mem}^{(2)}(\omega_3; \omega_1, \omega_2) : \mathbf{E}(\omega_1)\mathbf{H}(\omega_2), \end{aligned} \quad (1.2)$$

where ‘:’ implies a tensor inner product between the rank-3 second-order susceptibility tensors and the field vectors, and $\omega_3 = \omega_1 + \omega_2$. While the nature of optical magnetism in natural materials usually suppresses all terms except $\chi_{eee}^{(2)}$, this is not the case in metamaterials, whose structurally-induced magnetic moments can be equal in strength, or even stronger, than their electric counterparts. However, relating such a complex series of effective second-order susceptibilities to the microscopic metamaterial structure is not a trivial exercise. Thus, the goal of this section is to find a set of intuitive and general expressions to give insight into this relationship.

Let us consider a typical metamaterial, composed of dielectric and metallic inclusions arranged periodically on a cubic lattice, as conceptually illustrated in Fig. 1.1. The metamaterial itself is thus completely described by a dielectric function $\varepsilon(\mathbf{r})$, periodic along all three cartesian axes with lattice constant a . For the following analysis, it is instructive to take $\varepsilon(\mathbf{r})$ to be purely real, i.e. lossless. While this is

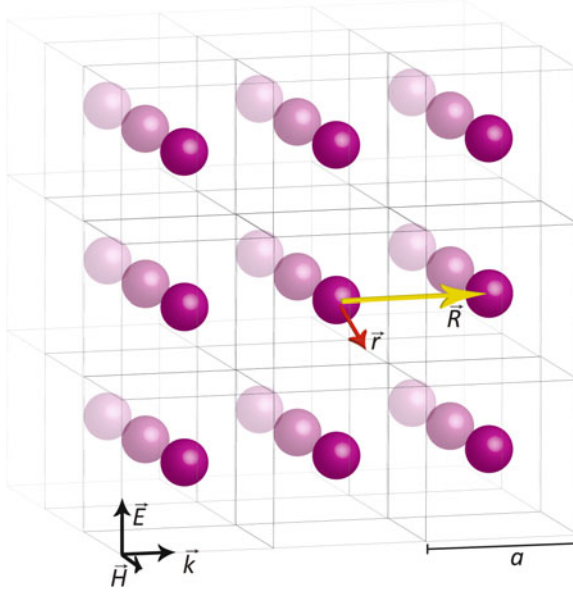


Fig. 1.1 Schematic of a cubic metamaterial lattice, indicating the microscopic position vector \mathbf{r} and macroscopic lattice vector \mathbf{R} . By equating coupled mode expressions on the discrete metamaterial lattice to that in a continuous, homogenized medium, we can arrive at a set of eight expressions for the eight effective second-order susceptibilities

clearly a poor approximation for most metamaterials of interest, the expressions that follow are still highly useful for yielding an intuitive understanding of the effective metamaterial properties, as well as probing some typical symmetries. In this limit we are free to decompose the total fields inside the metamaterial into a summation of Bloch modes, such that

$$\mathbf{E} = \sum_{\mu} A_{\mu} \mathbf{e}_{\mu}(\mathbf{r}) e^{i\mathbf{k}_{\mu} \cdot \mathbf{r} - i\omega_{\mu} t} \text{ and } \mathbf{H} = \sum_{\mu} A_{\mu} \mathbf{h}_{\mu}(\mathbf{r}) e^{i\mathbf{k}_{\mu} \cdot \mathbf{r} - i\omega_{\mu} t}, \quad (1.3)$$

where the μ label includes mode number, frequency, direction, and polarization. Since the repeat distance for elements forming a metamaterial is generally assumed to be much smaller than the wavelengths of interest, propagation is usually dominated by the Bloch mode with the smallest wavevector, often called the fundamental Bloch mode. This situation can be understood conceptually by imagining transmission and reflection from a single plane of the metamaterial, for which all higher order modes beyond the fundamental cannot propagate in free-space; that is, all of the diffractive beams are evanescent. So long as the coupling between adjacent metamaterial elements is relatively weak and is mostly dipolar, only the forward and backward propagating fundamental Bloch modes along a particular axis will contribute significantly to our analysis.

By describing our metamaterial in terms of these fundamental Bloch modes, we can quite naturally describe the perturbative effect of a nonlinear polarization via coupled mode theory, in perfect analogy to nonlinear waveguides [17]. For example, we can describe three waves with frequencies ω_1 , ω_2 , and $\omega_3 = \omega_1 + \omega_2$ propagating along the z -axis in the unperturbed case according to

$$\mathbf{E}(\omega_n) = A_n \mathbf{e}_n(\mathbf{r}) e^{ik_n z} + A_{-n} \mathbf{e}_n^*(\mathbf{r}) e^{-ik_n z}, \quad (1.4)$$

$$\mathbf{H}(\omega_n) = A_n \mathbf{h}_n(\mathbf{r}) e^{ik_n z} - A_{-n} \mathbf{h}_n^*(\mathbf{r}) e^{-ik_n z}, \quad (1.5)$$

for $n = 1, 2, 3$, where we have used Bloch mode symmetries and our freedom in selecting the relative phase of the Bloch functions to impose $\mathbf{e}_n(\mathbf{r}) = \mathbf{e}_{-n}(\mathbf{r})^*$ and $\mathbf{h}_n(\mathbf{r}) = -\mathbf{h}_{-n}(\mathbf{r})^*$. Now, assume that the metamaterial possesses a local second-order electric nonlinearity described by $\bar{\chi}_{\text{loc}}^{(2)}(\mathbf{r})$ with the same cubic periodicity. As a first step, consider the nonlinear polarization arising from the product of the *forward* propagating fields at ω_1 and ω_2 and allow the mode amplitude A_3 to vary in space. We can treat the nonlinearity as a perturbation to the fundamental Bloch modes. In the formalism of coupled mode theory, we can expect to find expressions relating the spatial rate of change of one amplitude over one lattice vector \mathbf{R} to the set of driving amplitudes, as in

$$\frac{\partial A_3}{\partial z}(\mathbf{R}) = i\Gamma A_1(\mathbf{R}) A_2(\mathbf{R}) e^{i(k_1+k_2-k_3)\hat{z}\cdot\mathbf{R}}, \quad (1.6)$$

through a proportionality constant Γ , called the coupling coefficient. While the formal derivation of this coupling coefficient, given by

$$\Gamma = \frac{\omega_3}{a^3} \iiint_{V_0} \left(\bar{\chi}_{\text{loc}}^{(2)}(\mathbf{r}) : \mathbf{e}_1(\mathbf{r}) \mathbf{e}_2(\mathbf{r}) \cdot \mathbf{e}_3^*(\mathbf{r}) e^{i(k_1+k_2-k_3)z} \right) dV, \quad (1.7)$$

can be found in [8], it can be simply understood as a volume average over the interacting fields within the nonlinear medium, and is very reminiscent of the coupling coefficients derived for standard nonlinear waveguides. Clearly, for a complete description, we must consider all possible products of forward and backward fields, generating in turn both forward and backward waves at ω_3 . However, each contribution will share a similar form to (1.6), and so they are suppressed for brevity.

Analogous expressions can be derived for a homogeneous medium, as a continuous function of position vector \mathbf{r} . However, for the sake of generality, the homogeneous medium must take into account all eight nonlinear susceptibilities in (1.1) and (1.2). By equating the discrete and continuous descriptions, three-wave mixing in a metamaterial can be homogenized, yielding expressions for the eight effective nonlinear susceptibility tensors. If we neglect spatial dispersion, i.e. $|k_n a| \ll 1$, then these expressions can be written in closed form, [8]

$$\chi_{eee}^{(2)}(\omega_3; \omega_1, \omega_2) = \frac{1}{a^3} \iiint dV \left[\bar{\bar{\chi}}_{\text{loc}}^{(2)}(\mathbf{r}) : \theta_1(\mathbf{r})\theta_2(\mathbf{r}) \cdot \theta_3(\mathbf{r}) \right], \quad (1.8)$$

$$\chi_{emm}^{(2)}(\omega_3; \omega_1, \omega_2) = \frac{-1}{a^3} \iiint dV \left[\bar{\bar{\chi}}_{\text{loc}}^{(2)}(\mathbf{r}) : \phi_1(\mathbf{r})\phi_2(\mathbf{r}) \cdot \theta_3(\mathbf{r}) \right], \quad (1.9)$$

$$\chi_{eem}^{(2)}(\omega_3; \omega_1, \omega_2) = \frac{i}{a^3} \iiint dV \left[\bar{\bar{\chi}}_{\text{loc}}^{(2)}(\mathbf{r}) : \theta_1(\mathbf{r})\phi_2(\mathbf{r}) \cdot \theta_3(\mathbf{r}) \right], \quad (1.10)$$

$$\chi_{eme}^{(2)}(\omega_3; \omega_1, \omega_2) = \frac{i}{a^3} \iiint dV \left[\bar{\bar{\chi}}_{\text{loc}}^{(2)}(\mathbf{r}) : \phi_1(\mathbf{r})\theta_2(\mathbf{r}) \cdot \theta_3(\mathbf{r}) \right], \quad (1.11)$$

$$\chi_{mmm}^{(2)}(\omega_3; \omega_1, \omega_2) = \frac{i}{a^3} \iiint dV \left[\bar{\bar{\chi}}_{\text{loc}}^{(2)}(\mathbf{r}) : \phi_1(\mathbf{r})\phi_2(\mathbf{r}) \cdot \phi_3(\mathbf{r}) \right], \quad (1.12)$$

$$\chi_{mee}^{(2)}(\omega_3; \omega_1, \omega_2) = \frac{-i}{a^3} \iiint dV \left[\bar{\bar{\chi}}_{\text{loc}}^{(2)}(\mathbf{r}) : \theta_1(\mathbf{r})\theta_2(\mathbf{r}) \cdot \phi_3(\mathbf{r}) \right], \quad (1.13)$$

$$\chi_{mme}^{(2)}(\omega_3; \omega_1, \omega_2) = \frac{1}{a^3} \iiint dV \left[\bar{\bar{\chi}}_{\text{loc}}^{(2)}(\mathbf{r}) : \phi_1(\mathbf{r})\theta_2(\mathbf{r}) \cdot \phi_3(\mathbf{r}) \right], \quad (1.14)$$

$$\chi_{mem}^{(2)}(\omega_3; \omega_1, \omega_2) = \frac{1}{a^3} \iiint dV \left[\bar{\bar{\chi}}_{\text{loc}}^{(2)}(\mathbf{r}) : \theta_1(\mathbf{r})\phi_2(\mathbf{r}) \cdot \phi_3(\mathbf{r}) \right], \quad (1.15)$$

where the volume integrals are taken over a single unit-cell. The quantities

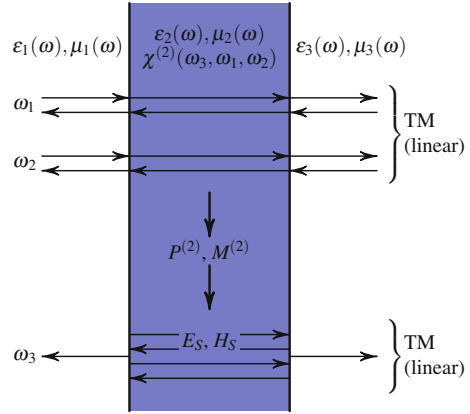
$$\theta_n(\mathbf{r}) = \text{Re} \left[\frac{\mathbf{e}_n(\mathbf{r})}{\tilde{\epsilon}_n} e^{ik_n z} \right] \quad \text{and} \quad \phi_n(\mathbf{r}) = \text{Im} \left[\frac{\mathbf{e}_n(\mathbf{r})}{\tilde{h}_n} e^{ik_n z} \right]$$

represent the inhomogeneous local electric fields induced in response to macroscopic, or ‘homogeneous’, electric fields $\tilde{\epsilon}_n$ and magnetic fields \tilde{h}_n , respectively. Qualitatively, these expressions imply that any of the eight fundamentally distinct nonlinear tensors, and any of the tensors’ individual elements, can be supported in metamaterial composites with no intrinsic magnetic properties, provided that the metamaterial supports sufficient overlap of the induced fields in the nonlinear element. An analogous set of expressions can be derived for the different tensor elements, or for the third-order susceptibilities [8].

1.3 Effective Nonlinear Susceptibilities: Transfer Matrix Method

The previous section presents a method to determine the effective nonlinear susceptibilities of lossless metamaterials by averaging the fields over a simulated unit cell, arriving at closed form solutions that can provide insight for nonlinear metamaterial design. The field averaging approach, however, requires knowledge of the fundamental and harmonic fields at all points throughout the volume of a unit cell of an infinitely periodic medium. An alternative approach uses the waves scattered from a sample of finite thickness to infer the effective linear and nonlinear susceptibilities. The advantage of this scattering (or S-) parameter retrieval is that the wave reflected and transmitted from a finite-thickness sample can be measured

Fig. 1.2 Schematic representation of the calculation of 3 wave mixing in a slab of homogeneous nonlinear material between two semi-infinite linear media: (1) the distribution of waves at ω_1 and ω_2 is calculated using a linear transfer matrix approach; (2) the nonlinear polarization is calculated; and (3) the wave generated at ω_3 is calculated using a linear transfer matrix approach



experimentally, rendering S-parameters retrieval applicable to simulation and experiment alike. Moreover, no restrictions on the geometry or composition of the metamaterial elements are required in the S-parameters method, allowing lossy samples to be investigated.

For linear retrievals, only two complex parameters—the effective permittivity and permeability—need be determined. They can be determined using two independent simulation or experimental complex results, usually the reflection and the transmission of the metamaterial. In the nonlinear case, a larger number of effective parameters must be determined and, therefore, a larger number of independent simulations or experiments must be performed. However, as we will see, the nonlinear retrieval is simpler in some aspects, ultimately involving the solution of a linear system of equations. In this section, we will first summarize how to calculate the nonlinear wave generated by the mixing of two or more waves in a homogeneous nonlinear slab and then we will show how to solve the inverse problem.

We first consider the case of waves normally incident on a slab of homogeneous material with known linear and nonlinear properties, situated between two semi-infinite linear media, as illustrated in Fig. 1.2. In the non-depleted pump approximation, the nonlinear process is sufficiently weak that the generated fields do not significantly impact the incident waves. Therefore, we can first calculate the field distribution of the incident waves by solving the wave equation assuming only the linear properties of the slab. We then calculate the nonlinear polarization, and finally calculate the generated waves [1].

For the transfer matrix formalism, it is useful to form two-element vectors from the complex coefficients of the forward and backward plane waves, which in region i are $E_i^\pm(\omega_n, z) = E_i^\pm(\omega_n) \exp[-i(\omega_n t \mp kz)]$, where the positive and negative superscripts indicate waves propagating in the forward and backward directions, respectively. In region i , the electric and magnetic fields at frequency ω_n can thus be decomposed into the vectors

$$\mathbf{E}_i(\omega_n) = \begin{bmatrix} E_i^+(\omega_n) \\ E_i^-(\omega_n) \end{bmatrix}, \quad \text{or} \quad \mathbf{H}_i(\omega_n) = \begin{bmatrix} H_i^+(\omega_n) \\ H_i^-(\omega_n) \end{bmatrix}. \quad (1.16)$$

In the linear case, the plane wave coefficients for any of the dependent waves can be calculated from the incident waves ($E_1^+(\omega_n)$ and $E_3^-(\omega_n)$, or $H_1^+(\omega_n)$ and $H_3^-(\omega_n)$) by applying the well-established transfer matrix formalism [5]. With all coefficients known, the fields can then be calculated at any position in the system. In particular, we can calculate $\mathbf{E}_2(\omega_{1,2})$ and $\mathbf{H}_2(\omega_{1,2})$, the fields inside the slab, necessary to compute wave-mixing processes.

To keep the number of terms tractable, we will consider the case of a second order nonlinearity, but the approach presented here can easily be extended to arbitrary order nonlinearities. In the present case, the nonlinear polarization and magnetization are representable as a sum of contributions from eight different terms associated with eight nonlinear susceptibilities. Since the fields are decomposed into forward and backward propagating waves, we can separate the nonlinear polarization and magnetization into two different sums corresponding to the product of waves propagating in the same or in opposite directions and associated with wavevectors $k_{\text{sum}} = k_1 + k_2$ and $k_{\text{diff}} = k_1 - k_2$, respectively. Thus, in the vector notation of (1.16), the nonlinear polarization is the sum of

$$\begin{aligned} \mathbf{P}_{\text{sum}} = & \frac{1}{2} \chi_{eee}^{(2)} \mathbf{E}_2(\omega_1) \mathbf{E}_2^T(\omega_2) + \frac{1}{2} \chi_{eem}^{(2)} \mathbf{E}_2(\omega_1) \mathbf{H}_2^T(\omega_2) \\ & + \frac{1}{2} \chi_{eme}^{(2)} \mathbf{H}_2(\omega_1) \mathbf{E}_2^T(\omega_2) + \frac{1}{2} \chi_{emm}^{(2)} \mathbf{H}_2(\omega_1) \mathbf{H}_2^T(\omega_2) \end{aligned} \quad (1.17)$$

and

$$\begin{aligned} \mathbf{P}_{\text{diff}} = & \frac{1}{2} \chi_{eee}^{(2)} \mathbf{E}_2(\omega_1) (F \mathbf{E}_2(\omega_2))^T + \frac{1}{2} \chi_{eem}^{(2)} \mathbf{E}_2(\omega_1) (F \mathbf{H}_2(\omega_2))^T \\ & + \frac{1}{2} \chi_{eme}^{(2)} \mathbf{H}_2(\omega_1) (F \mathbf{E}_2(\omega_2))^T + \frac{1}{2} \chi_{emm}^{(2)} \mathbf{H}_2(\omega_1) (F \mathbf{H}_2(\omega_2))^T \end{aligned} \quad (1.18)$$

while the nonlinear magnetization is the sum of

$$\begin{aligned} \mu_0 \mathbf{M}_{\text{sum}} = & \frac{1}{2} \chi_{mee}^{(2)} \mathbf{E}_2(\omega_1) \mathbf{E}_2^T(\omega_2) + \frac{1}{2} \chi_{mem}^{(2)} \mathbf{E}_2(\omega_1) \mathbf{H}_2^T(\omega_2) \\ & + \frac{1}{2} \chi_{mme}^{(2)} \mathbf{H}_2(\omega_1) \mathbf{E}_2^T(\omega_2) + \frac{1}{2} \chi_{mmm}^{(2)} \mathbf{H}_2(\omega_1) \mathbf{H}_2^T(\omega_2) \end{aligned} \quad (1.19)$$

and

$$\begin{aligned} \mu_0 \mathbf{M}_{\text{diff}} = & \frac{1}{2} \chi_{mee}^{(2)} \mathbf{E}_2(\omega_1) (F \mathbf{E}_2(\omega_2))^T + \frac{1}{2} \chi_{mem}^{(2)} \mathbf{E}_2(\omega_1) (F \mathbf{H}_2(\omega_2))^T \\ & + \frac{1}{2} \chi_{mme}^{(2)} \mathbf{H}_2(\omega_1) (F \mathbf{E}_2(\omega_2))^T + \frac{1}{2} \chi_{mmm}^{(2)} \mathbf{H}_2(\omega_1) (F \mathbf{H}_2(\omega_2))^T, \end{aligned} \quad (1.20)$$

where

$$F = \begin{bmatrix} 0 & 1 \\ 1 & 0 \end{bmatrix}, \quad (1.21)$$

effectively flipping the vector it multiplies upside down.

In the non depleted pump approximation, the nonlinear polarizations and magnetizations can be treated as source terms at $\omega_3 = \omega_1 + \omega_2$. These are associated with source electric and magnetic fields

$$\mathbf{E}_{s,\text{sum}} = \frac{\mathbf{P}_{\text{sum}}\mu_{r,2}(\omega_3)}{n_{s,\text{sum}}^2 - n_2^2(\omega_3)}, \quad \mathbf{E}_{s,\text{diff}} = \frac{\mathbf{P}_{\text{diff}}\mu_{r,2}(\omega_3)}{n_{s,\text{diff}}^2 - n_2^2(\omega_3)}, \quad (1.22)$$

$$\mathbf{H}_{s,\text{sum}} = \frac{\mathbf{M}_{\text{sum}}\varepsilon_{r,2}(\omega_3)}{n_{s,\text{sum}}^2 - n_2^2(\omega_3)}, \quad \text{and} \quad \mathbf{H}_{s,\text{diff}} = \frac{\mathbf{M}_{\text{diff}}\varepsilon_{r,2}(\omega_3)}{n_{s,\text{diff}}^2 - n_2^2(\omega_3)}. \quad (1.23)$$

Using the method developed by Bethune [1], a series of boundary conditions can be used to derive transfer matrices relating these source fields to the fields at ω_3 generated on both sides of the slab, $E_1^-(\omega_3)$ and $E_3^+(\omega_3)$, or $H_1^-(\omega_3)$ and $H_3^+(\omega_3)$.

At this point, it is important to note that the nonlinear polarizations—and therefore the waves generated at ω_3 —depend nonlinearly on the applied fields, but linearly on the nonlinear susceptibilities. Using this to our advantage, we can build a linear system of equations to retrieve the effective nonlinear susceptibilities of a metamaterial. For example, if only one nonlinear susceptibility is present, one can determine it by calculating what would be any of $E_1^-(\omega_3)$, $E_3^+(\omega_3)$, $H_1^-(\omega_3)$, or $H_3^+(\omega_3)$ if the nonlinear susceptibility were unity, and comparing that result with the actual generation from simulation or experiment [4, 7]. When many nonlinear susceptibilities are present, the situation is just slightly more complex [9], leading to a system of linear equations.

To retrieve the effective nonlinear susceptibilities, one must:

1. Determine the effective linear properties of the matematerial at all frequencies involved using the standard retrieval approach.
2. Choose a series of independant simulation or experiment conditions giving as many results as there are effective nonlinear susceptibilities. For 3-wave mixing, if the waves generated in media 1 and 3 are both measured, 4 simulations or experiments are necessary for a total of 8 complex results—Table 1.1 shows two possible series of conditions.
3. Calculate the amplitude of the wave generated at ω_3 in media 1 and 3 using the predetermined linear effective properties and the transfer matrix approach for every susceptibility being separately unity and for all conditions.
4. Simulate or experimentally determine the amplitude of the nonlinearly generated wave in media 1 and 3 for the same series of conditions.
5. Solve the linear system of equations

Table 1.1 Two possible choices of 4 independant simulation or experiment conditions to determine all effective nonlinear susceptibilities for 3-wave mixing

Condition	Choice 1				Choice 2			
	$E_1^+(\omega_1)$ (V/m)	$E_3^-(\omega_1)$ (V/m)	$E_1^+(\omega_2)$ (V/m)	$E_3^-(\omega_2)$ (V/m)	$E_1^+(\omega_1)$ (V/m)	$E_3^-(\omega_1)$ (V/m)	$E_1^+(\omega_2)$ (V/m)	$E_3^-(\omega_2)$ (V/m)
A	1	0	1	0	+1	+1	+1	+1
B	1	0	0	1	+1	+1	+1	-1
C	0	1	1	0	+1	-1	+1	+1
D	0	1	0	1	+1	-1	+1	-1

The first choice might be easier to implement experimentally. The second choice has the advantage of creating standing waves with zeros or maxima in the electric and magnetic fields favoring selected nonlinearities. For experiments the amplitude of the fields should be scaled such that the nonlinear effect produces a good signal to noise ratio, without violating the non-depleted pump approximation

$$\begin{bmatrix}
 E_{1,A}^- \left| \chi_{eee}^{(2)}=1 \right. & E_{1,A}^- \left| \chi_{eem}^{(2)}=1 \right. & E_{1,A}^- \left| \chi_{eme}^{(2)}=1 \right. & E_{1,A}^- \left| \chi_{emm}^{(2)}=1 \right. & \cdots \\
 E_{3,A}^+ \left| \chi_{eee}^{(2)}=1 \right. & E_{3,A}^+ \left| \chi_{eem}^{(2)}=1 \right. & E_{3,A}^+ \left| \chi_{eme}^{(2)}=1 \right. & E_{3,A}^+ \left| \chi_{emm}^{(2)}=1 \right. & \cdots \\
 E_{1,B}^- \left| \chi_{eee}^{(2)}=1 \right. & E_{1,B}^- \left| \chi_{eem}^{(2)}=1 \right. & E_{1,B}^- \left| \chi_{eme}^{(2)}=1 \right. & E_{1,B}^- \left| \chi_{emm}^{(2)}=1 \right. & \cdots \\
 E_{3,B}^+ \left| \chi_{eee}^{(2)}=1 \right. & E_{3,B}^+ \left| \chi_{eem}^{(2)}=1 \right. & E_{3,B}^+ \left| \chi_{eme}^{(2)}=1 \right. & E_{3,B}^+ \left| \chi_{emm}^{(2)}=1 \right. & \cdots \\
 \vdots & \vdots & \vdots & \vdots & \ddots
 \end{bmatrix}
 \begin{bmatrix}
 \chi_{eee}^{(2)} \\
 \chi_{eem}^{(2)} \\
 \chi_{eme}^{(2)} \\
 \chi_{emm}^{(2)} \\
 \chi_{mee}^{(2)} \\
 \chi_{mem}^{(2)} \\
 \chi_{mme}^{(2)} \\
 \chi_{mmm}^{(2)}
 \end{bmatrix}
 =
 \begin{bmatrix}
 E_{1,A}^- \\
 E_{3,A}^+ \\
 E_{1,B}^- \\
 E_{3,B}^+ \\
 E_{1,C}^- \\
 E_{3,C}^+ \\
 E_{1,D}^- \\
 E_{3,D}^+
 \end{bmatrix}, \quad (1.24)$$

where the frequency dependence has been omitted for brevity. The matrix contains the results of the transfer matrix calculations for homogeneous slabs with a single nonlinearity for all conditions, the vector on the right hand side contains the results of the simulations or experiments on the metamaterial in the same conditions, and the vector on the left hand side contains the effective susceptibilities to be determined.

1.4 Symmetries and Spatial Dispersion

At this point, it is useful to consider the effective nonlinear properties from a symmetry standpoint. First, simply by considering the polar and axial natures of the electric and magnetic field vectors, we see that the eight nonlinearities separate naturally into polar and axial tensors. Specifically, the tensors $\bar{\chi}_{eee}^{(2)}$, $\bar{\chi}_{mme}^{(2)}$, $\bar{\chi}_{emm}^{(2)}$, and $\bar{\chi}_{mem}^{(2)}$, involving an even number of magnetic fields, are polar, whereas the other four are axial. We would thus expect that certain internal symmetries of a given metamaterial, then, would favor one group of tensors over another.

For example, consider a metamaterial whose linear properties are centrosymmetric, that is, for some choice of origin $\varepsilon(\mathbf{r}) = \varepsilon(-\mathbf{r})$ for all \mathbf{r} within the unit-cell. Such

symmetry is a good approximation for regular arrangements of symmetric nanoparticles and many circuit-based metamaterials like dual-split SRRs and ELCs. It is worth noting that we are not referring to the crystal symmetry of the local materials, at least some of which must be non-centrosymmetric to support a $\chi_{\text{loc}}^{(2)}$, but rather the structural symmetry of the metamaterial unit-cell, which depends on the relative arrangement of the constituent materials and inclusions. As such, even though the anisotropy of the nonlinear elements, as well as the presence of substrates will, strictly speaking, break the inversion symmetry, it is instructive to consider the structural symmetry of the inclusion as the dominant force influencing the effective properties. In any case, for a centrosymmetric unit-cell, we know from Bloch theory that a similar symmetry is enforced in the local fields, or $\mathbf{e}_n(\mathbf{r}) = \mathbf{e}_n(-\mathbf{r})^*$. From the definitions of θ and ϕ , we see that this in turn implies that $\theta(\mathbf{r})$ is an even function of \mathbf{r} , while $\phi(\mathbf{r})$ is odd. Clearly, these symmetry properties will have a strong impact on which of the effective nonlinearities are dominant. If the nonlinear properties are similarly centrosymmetric, i.e. $\chi_{\text{loc}}^{(2)}(\mathbf{r}) = \chi_{\text{loc}}^{(2)}(-\mathbf{r})$, then the integrands in the expressions for the axial nonlinear tensors are odd functions of \mathbf{r} and therefore the axial nonlinear tensors vanish identically. If, on the other hand, the material is poled in such a way that the local nonlinear properties are anti-symmetric, $\chi_{\text{loc}}^{(2)}(\mathbf{r}) = -\chi_{\text{loc}}^{(2)}(-\mathbf{r})$, then the polar nonlinear tensors vanish. These cases are illustrated in Fig. 1.3a and b, respectively.

At microwave frequencies, where circuit elements such as varactor diodes are often used as the nonlinear inclusions, it is simple to create metamaterial structures possessing selected symmetries in the nonlinear properties, giving access to any of the eight nonlinear susceptibilities. At optical frequencies, however, local electric nonlinearities are often introduced by using a nonlinear crystal as a substrate

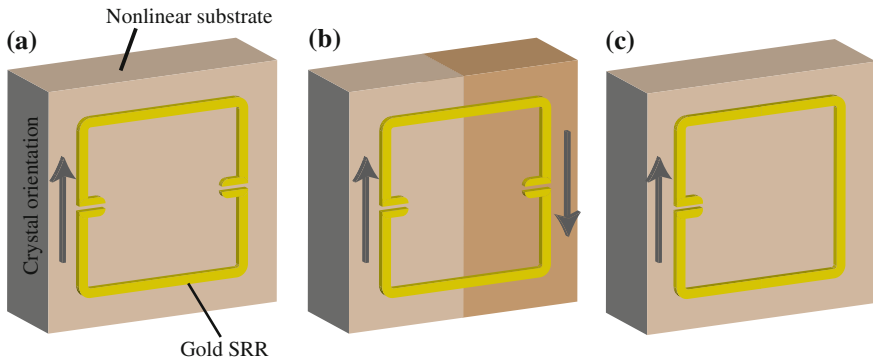


Fig. 1.3 Illustration of symmetries in nonlinear metamaterials. **a** A centrosymmetric inclusion, the double-gap SRR, placed over a uniform nonlinear substrate for maximizing the polar second-order susceptibility tensors. **b** A centrosymmetric inclusion placed over an anti-symmetric nonlinear substrate for maximizing the axial second-order susceptibility tensors. **c** A non-centrosymmetric inclusion placed over a uniform substrate excludes neither polar nor axial second-order susceptibility tensors

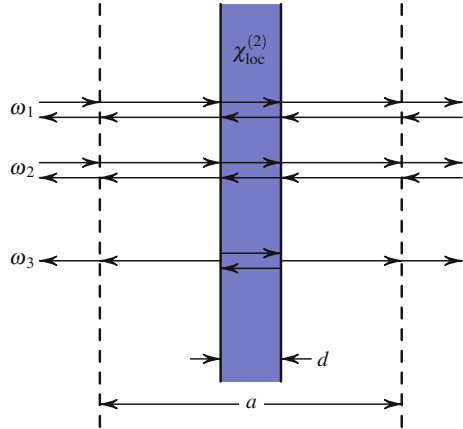
or embedding matrix. While a nonlinear crystal as a whole can be aligned along a particular axis, enforcing local directionality in a bulk medium or substrate can be very difficult, especially on the length scales that would be required in a metamaterial. This implies that, at optical frequencies, the class of nonlinear metamaterials composed of centrosymmetric inclusions will tend to support nonlinear processes through effectively polar nonlinear tensors. Accessing the axial tensors requires non-centrosymmetric inclusions, such as the single-gap SRR shown in Fig. 1.3c, which is known to support nonlinearities of the type $\chi_{mmm}^{(2)}$ [3].

Related to these symmetry considerations is the phenomena of spatial dispersion. In the linear properties of metamaterials, it is often the case that spatial dispersion, resulting from the non-negligible lattice dimensions, will lead to artifacts in the effective linear properties other than the principal resonance [13]. Similar effects show up in the nonlinear properties when the lattice constant-to-wavelength ratio is sufficiently large. As an example, let us consider the simple case of a thin slab of nonlinear material possessing only a $\chi_{eee}^{(2)}$ nonlinear susceptibility periodically embedded in dielectric, as in Fig. 1.4. In the long wavelength limit, all nonlinearities vanish with the exception of $\chi_{eee}^{(2)}(\omega_3; \omega_1, \omega_2) = \frac{d}{a} \chi_{loc}^{(2)}$, in agreement with previous studies of composite nonlinear media [12]. Since the linear and nonlinear properties possess inversion symmetry, the four axial nonlinear susceptibilities are identically zero for *all* wavelengths. This leaves us with a system of four equations and four unknown polar nonlinear susceptibilities. In the limit $d \ll a$, these expressions can be solved to leading order in $k_i a$,

$$\chi_{eee}^{(2)} = \left[1 - \frac{1}{8} a^2 (k_1^2 + k_2^2 + k_3^2) \right] \frac{d}{a} \chi_{loc}^{(2)} \quad (1.25)$$

$$\chi_{emm}^{(2)} = +Z_1 Z_2 \left(\frac{1}{12} a^2 k_1 k_2 \right) \frac{d}{a} \chi_{loc}^{(2)} = +Z_0^2 \left(\frac{\pi^2}{3} \frac{a^2}{\lambda_1 \lambda_2} \right) \frac{d}{a} \chi_{loc}^{(2)} \quad (1.26)$$

Fig. 1.4 A simple unit cell that can be used to demonstrate the effect of spatial dispersion on the effective nonlinear susceptibilities. This unit cell consists of a slab of thickness d containing an intrinsic nonlinearity centered inside the unit cell of thickness a . For simplicity, all linear properties are considered to be those of vacuum



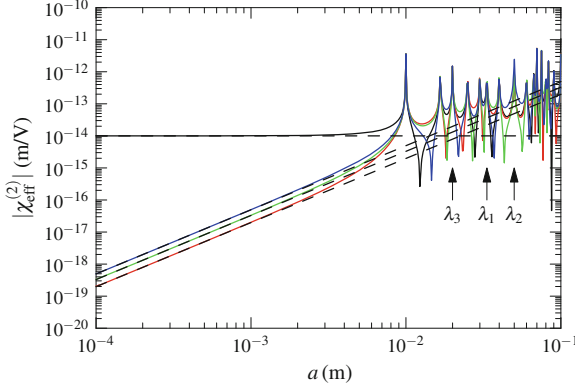


Fig. 1.5 The effective nonlinear susceptibilities, $\chi_{eee}^{(2)}$ (black), χ_{emmm}/Z_0^2 (red), χ_{mem}/Z_0^2 (green), and χ_{mme}/Z_0^2 (blue) for the unit cell presented in Fig. 1.4, $f_1 = 9$ GHz, $f_2 = 6$ GHz, and $f_3 = f_1 + f_2 = 15$ GHz determined using the transfer matrix approach. Arrows indicate the wavelengths $\lambda_n = c/f_n$ involved in 3-wave mixing. The dashed lines correspond to the prediction of approximate (1.25–1.28)

$$\chi_{mme}^{(2)} = -Z_1 Z_3 \left(\frac{1}{12} a^2 k_1 k_3 \right) \frac{d}{a} \chi_{loc}^{(2)} = -Z_0^2 \left(\frac{\pi^2}{3} \frac{a^2}{\lambda_1 \lambda_3} \right) \frac{d}{a} \chi_{loc}^{(2)} \quad (1.27)$$

$$\chi_{mem}^{(2)} = -Z_2 Z_3 \left(\frac{1}{12} a^2 k_2 k_3 \right) \frac{d}{a} \chi_{loc}^{(2)} = -Z_0^2 \left(\frac{\pi^2}{3} \frac{a^2}{\lambda_2 \lambda_3} \right) \frac{d}{a} \chi_{loc}^{(2)} \quad (1.28)$$

where $\lambda_n = 2\pi c/\omega_n$ is the wavelength in free-space, Z_n is the effective impedance of the metamaterial at wavelength λ_n , and Z_0 is the impedance of vacuum. Thus, spatial dispersion manifests itself in the nonlinear susceptibilities of the same polar/axial nature, proportional to the square of the lattice constant-to-wavelength ratio.

Figure 1.5 shows the effect of spatial dispersion on the retrieved parameters as calculated using the transfer matrix approach as well as using the approximate formula just derived. When the unit cell thickness is much smaller than all wavelengths involved, the intrinsic nonlinearity dominates. Nonlinearities of the same polar/axial nature are also present, but tend toward 0 when $a \rightarrow 0$ while nonlinearities of the other polar/axial nature are identically 0. Following the same rule of thumb used when determining the linear effective properties, the effect of spatial dispersion can be neglected when the unit cell size is smaller than approximately a tenth of all wavelengths involved.

The unit cell considered here is obviously much simpler than would be expected for any practical metamaterial, but cleanly illustrates the effects of symmetry and spatial dispersion, which will generally impact all nonlinear metamaterial constructs. Moreover, analogous selection rules can be derived for metamaterials belonging to a variety of symmetry classes; for example, the circular polarization selection rules for four-wave mixing in certain chiral metamaterials have been investigated both analytically and experimentally along similar lines of reasoning [10].

1.5 Application to Varactor-Loaded Split-Ring Resonators

The methods developed above can be applied in nonlinear metamaterial design. As an example, in this section we will apply them to varactor-loaded split-ring resonators (VLSRRs), which have been used as nonlinear metamaterials in the microwave range [11, 16]. They are obtained by adding a varactor diode, which has intrinsically large nonlinear response, inside the gap(s) of a SRR. Here, we will consider a SRR with two gaps, like that of Fig. 1.3, but instead of assuming the SRR is patterned on a nonlinear substrate, two varactors are used to introduce the desired nonlinearity. As shown in Fig. 1.6, the varactors can be inserted in the same direction (symmetric case), or in opposite directions (antisymmetric case), to favor different kinds of nonlinear susceptibilities.

Here, we consider the case of second harmonic generation. This is a particular case of 3-wave mixing where ω_1 and ω_2 are degenerate. Because of that, $\chi_{eem}^{(2)}$ and $\chi_{eme}^{(2)}$, as well as $\chi_{mem}^{(2)}$ and $\chi_{mme}^{(2)}$, are also degenerate. The VLSRR has been designed to have a resonance frequency of about 1 GHz. The pump wave is applied around the resonance frequency, while the harmonic is generated at twice that frequency. All simulations were performed using Comsol.

In the previous section, we gained some insight into determining which nonlinear susceptibilities should be favored in such a system using the coupled mode approach. However, for real materials with finite absorption, the assumptions of the coupled mode theory are violated and it cannot be used to provide quantitative evaluations. In this section, we therefore use the transfer matrix approach to obtain quantitative results and compare them to the predictions intuitively obtained from the coupled mode theory.

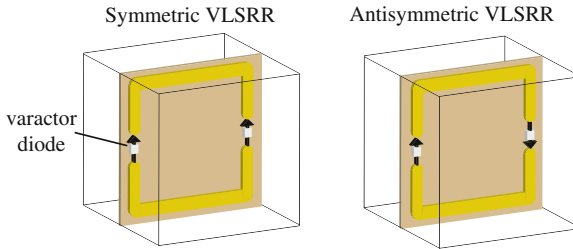


Fig. 1.6 Symmetric and antisymmetric VLSRRs

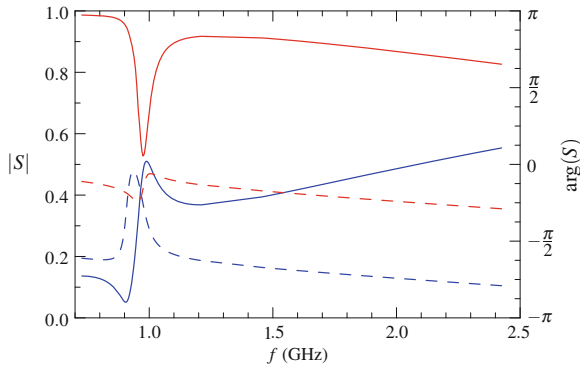


Fig. 1.7 S parameters of a dual gap VLSRR: amplitude (*continuous line*) and phase (*dashed line*) of S_{11} (*blue*) and S_{21} (*red*)

1.5.1 Linear Properties

The first step in the transfer matrix approach is to determine the effective linear properties of the metamaterial unit cell. The only difference between the symmetric and the antisymmetric unit cells is in the nonlinear response, and both therefore have the same linear properties. Figure 1.7 shows the amplitude and phase of the S parameters of the VLSRR determined over a range of frequencies covering both the pump and the harmonic frequencies.

Using the well-established retrieval method [2, 14, 15], the effective linear parameters of this structures were determined, and are shown in Fig. 1.8. It should be observed that this material shows a strong magnetic resonance while the electric response is essentially flat. The small *anti*-resonance in the permittivity is an artifact of spatial dispersion [13]. As shown in Fig. 1.9, it is also interesting to note that applied magnetic fields generate concentration of the electric field inside the gaps of the VLSRR and, therefore, important charges on the varactors. On the contrary, the coupling of the electric field mainly generates field concentration on the sides of the VLSRR, where no nonlinear material is present.

1.5.2 Nonlinear Properties

To determine the nonlinear properties of the VLSRR medium, a series of nonlinear simulations must be performed for various combinations of incident fields. For both the symmetric and antisymmetric VLSRR unit cells, the pump was applied either on the left (condition A), on the right (condition B), or on both sides (condition C) of the unit cell at once. Because of the degeneracy of some of the nonlinear susceptibilities, only three conditions are necessary to determine all six independent susceptibilities.

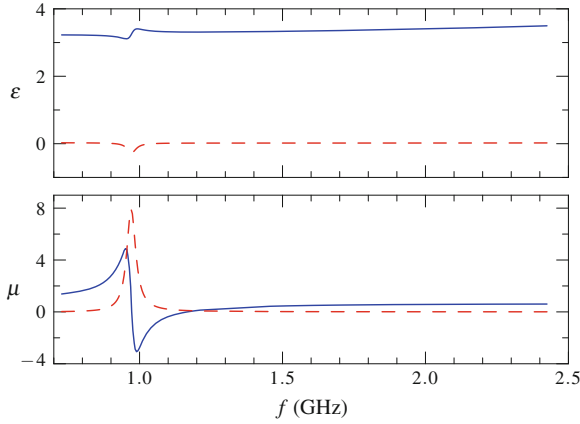


Fig. 1.8 Real (*continuous line*) and imaginary (*dashed line*) parts of the effective linear properties of a dual gap VLSRR

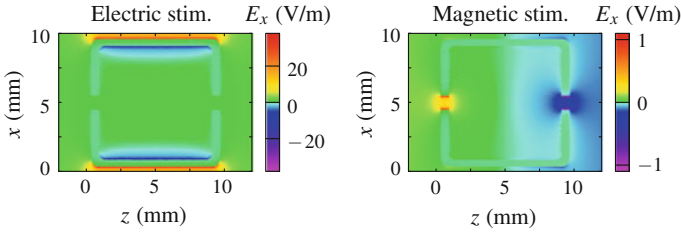


Fig. 1.9 Electric field pattern around the VLSRR for mainly electric (*left*) or magnetic (*right*) stimulation. In both cases, incident fields are applied at the resonance frequency from both sides of the VLSRR with the electric field polarized in the x axis and the magnetic field polarized in the y axis. To stimulate the VLSRR mainly with an electric (magnetic) field, the incident fields on both sides are applied in (anti-)phase creating a maximum (zero) of the electric field and a zero (maximum) of the magnetic field at the center of the unit cell

The applied fields are always 1 V/m. Figure 1.10 shows the amplitude and the phase of the second harmonic generated on the left and the right of the metamaterial.

Many observations can be made directly from these plots, the most obvious being that the symmetric unit cell generates a second harmonic that is almost perfectly in phase on both sides, while the antisymmetric unit cell generates a second harmonic that is approximately π out of phase on both sides of the metamaterial. If the magnetic field were plotted instead of the electric field, the inverse effect would be observed. This symmetry can be explained by the fact that the symmetric unit cell acts as an electric dipole source at the harmonic frequency, while the antisymmetric unit cell acts as a magnetic dipole source [6].

It can also be seen that conditions A and B give identical results, but with the amplitude and phase in the left and right media reversed. This behavior is to be expected for symmetric or antisymmetric unit cells since those two conditions are in fact totally equivalent.

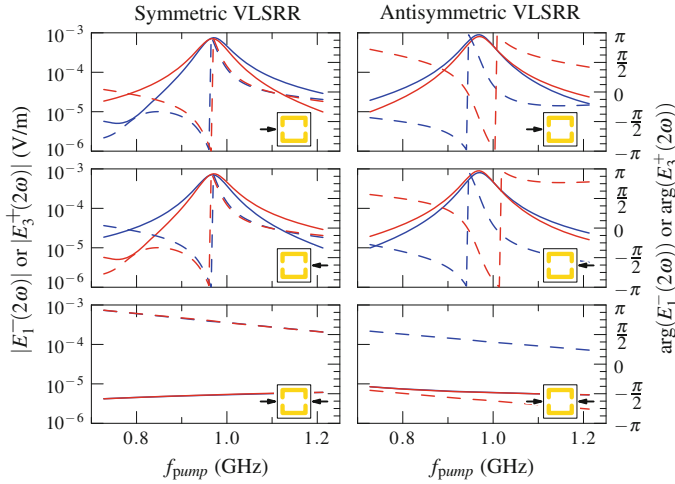


Fig. 1.10 Amplitude (continuous line) and phase (dashed line) of second harmonic generated on the left (blue) and the right (red) of the unit cell for symmetric (left) and antisymmetric (right) VLSRRs in three different conditions. The insets represent the incident fields in conditions A (top), B (middle), or C (bottom)

Finally, it can be seen that when the pump is applied in condition C, the second harmonic generation is suppressed. Since the pump is applied symmetrically in condition C, it creates a standing wave with node in the electric field and a zero in the magnetic field at the center of the unit cell. As shown above in Fig. 1.9, such a combination of incident fields does not generate a concentration of the electric field inside the gaps of the VLSRR, and we expect a weak nonlinear response.

The amplitude and phase of the generated second harmonic can be compared to how much would be generated if the nonlinear susceptibilities were individually unity. Using the transfer matrix approach of Bethune, all the elements of the matrix of (1.24) were calculated and the linear system of equation was solved to obtain the effective nonlinear susceptibilities shown in Fig. 1.11.

The dominant nonlinearity in the symmetric VLSRR is $\chi_{emm}^{(2)}$ while that of the antisymmetric VLSRR is $\chi_{mmm}^{(2)}$. In both cases, it is mainly the applied magnetic field that generates the second harmonic. This is related to the fact that field concentration in the gaps of the VLSRR is mainly generated by the applied magnetic field. When the varactors are in the symmetric orientation the unit cell acts as an electric dipole source at the harmonic frequency, while when the varactors are in the antisymmetric orientation the unit cell acts as a magnetic dipole source. The next two nonlinear susceptibilities in importance for both cases are those of the same symmetry group as the dominant nonlinearity. Their presence is probably for the most part an artifact of spatial dispersion. The three remaining nonlinearities belong to the opposite symmetry group, and are suppressed by several orders of magnitude, in agreement with the conclusions drawn earlier from the coupled mode theory.

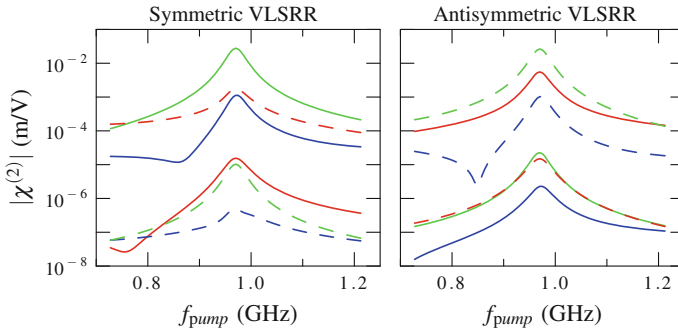


Fig. 1.11 Nonlinear susceptibility for symmetric (*left*) and antisymmetric (*right*) VLSRRs: $\chi_{eee}^{(2)}$ (blue), $\chi_{eem}^{(2)}$ (red), $\chi_{emm}^{(2)}$ (green), $\chi_{mee}^{(2)}/Z_0$ (blue, dashed), $\chi_{mem}^{(2)}/Z_0$ (red, dashed), and $\chi_{mmm}^{(2)}/Z_0$ (green, dashed)

1.6 Conclusion

Metamaterials offer an enormously expanded set of tools for the design of novel nonlinear optical media. With the inclusion of artificial magnetic response, which can readily be realized in artificially structured media, the number of potential nonlinear susceptibilities dramatically increases, allowing much more control over harmonic generation or wave mixing processes, as well as many other nonlinear phenomena. In this chapter, we have presented methods to design and evaluate general magnetoelectric nonlinear metamaterials, and have shown how the various nonlinear susceptibility terms can be understood in terms of symmetry arguments. The simple illustrations we have presented represent only a modest introduction to the subject of nonlinear magnetoelectric metamaterials, which hold great potential for new nonlinear physics and nonlinear device optimization.

Acknowledgments This work was supported by the Air Force Office of Scientific Research (Contract No. FA9550-09-1-0562).

References

1. D.S. Bethune, Optical harmonic generation and mixing in multilayer media: analysis using optical transfer matrix techniques. *J. Opt. Soc. Am. B* **6**(5), 910–916 (1989)
2. X. Chen, T.M. Grzegorzczuk, B.I. Wu, J. Pacheco Jr, J.A. Kong, Robust method to retrieve the constitutive effective parameters of metamaterials. *Phys. Rev. E* **70**, 016,608 (2004)
3. S. Larouche, A. Rose, E. Poutrina, D. Huang, D.R. Smith, Experimental determination of the quadratic nonlinear magnetic susceptibility of a varactor-loaded split ring resonator metamaterial. *Appl. Phys. Lett.* **97**, 011,109 (2010)
4. S. Larouche, D.R. Smith, A retrieval method for nonlinear metamaterials. *Opt. Commun.* **283**, 1621–1627 (2010)

5. P. Markoš, C.M. Soukoulis, *Wave Propagation: From Electrons to Photonic Crystals and Left-Handed Metaamaterials* (Princeton University Press, Princeton, 2008)
6. A. Rose, D. Huang, D.R. Smith, Demonstration of nonlinear magnetoelectric coupling in metamaterials. *Appl. Phys. Lett.* **101**, 051,103 (2012)
7. A. Rose, S. Larouche, D. Huang, E. Poutrina, D.R. Smith, Nonlinear parameter retrieval from three- and four-wave mixing in metamaterials. *Phys. Rev. E* **82**, 036,608 (2010)
8. A. Rose, S. Larouche, E. Poutrina, D.R. Smith, Nonlinear magnetoelectric metamaterials: Analysis and homogenization via a microscopic coupled-mode theory. *Phys. Rev. A* **86**, 033,816 (2012)
9. A. Rose, S. Larouche, D.R. Smith, Quantitative study of the enhancement of bulk nonlinearities in metamaterials. *Phys. Rev. A* **84**, 053,805 (2011)
10. A. Rose, D.A. Powell, I.V. Shadrivov, D.R. Smith, Y.S. Kivshar, Circular dichroism of four-wave mixing in nonlinear metamaterials. *Phys. Rev. B* **88**, 195,148 (2013)
11. I.V. Shadrivov, A.B. Kozyrev, D.W. van der Weide, Y.S. Kivshar, Nonlinear magnetic metamaterials. *Opt. Express* **16**(25), 20,266–20,271 (2008)
12. J.E. Sipe, R.W. Boyd, Nonlinear susceptibility of composite optical materials in the Maxwell Garnett model. *Phys. Rev. A* **46**(3), 1614–1629 (1992)
13. D.R. Smith, Analytic expressions for the constitutive parameters of magnetoelectric metamaterials. *Phys. Rev. E* **81**, 036,605 (2010)
14. D.R. Smith, S. Schultz, P. Markoš, C.M. Soukoulis, Determination of effective permittivity and permeability of metamaterials from reflection and transmission coefficients. *Phys. Rev. B* **65**, 195,104 (2002)
15. D.R. Smith, D.C. Vier, Th. Koschny, C.M. Soukoulis, Electromagnetic parameter retrieval from inhomogeneous metamaterials. *Phys. Rev. E* **71**, 036,617 (2005)
16. B. Wang, J. Zhou, Th. Koschny, C.M. Soukoulis, Nonlinear properties of split-ring resonators. *Opt. Express* **16**(20), 16,058–16,063 (2008)
17. A. Yariv, Coupled-mode theory for guided-wave optics. *IEEE J. Quantum Electron QE* **9**(9), 919–933 (1973)

Nonlinear, Tunable and Active Metamaterials

Shadrivov, I.V.; Lapine, M.; Kivshar, Y.S. (Eds.)

2015, XXII, 324 p. 158 illus., 126 illus. in color.,

Hardcover

ISBN: 978-3-319-08385-8